Large Contribution of Kilometer-Scale Snow Transport to Alpine Hydrology Constrained by Differentiable Modeling and Airborne Lidar

E. N. Boardman[1,2]

[1]Graduate Program of Hydrologic Sciences, University of Nevada, Reno, Reno, NV, USA

[2]Mountain Hydrology LLC, Reno, NV, USA

Corresponding author: Elijah N. Boardman (eli.boardman@mountainhydrology.com)

Key Points:

- A differentiable model of snow transport constrains the minimum seasonal flux required to explain lidar-based snow accumulation patterns.
- Extensive deep snow accumulation (3-9 times local snowfall, >0.01 km^2) requires mass-weighted mean contributing distances of 0.3 to 2.1 km.
- Interbasin snow transport can double the catchment area of first-order streams and can contribute 7% of water yield at the 100 km^2 scale.

Abstract

The farther you roll a snowball, the more snow is accumulated. How far must you roll a snowball to create a major alpine snow drift? From this analogy, I develop a framework using airborne lidar data and differentiable modeling to constrain the minimum seasonal transport flux needed to explain alpine snow accumulation patterns. In the Wind River Range, Wyoming, 100 m grid cells with 3-6 m SWE must accumulate snowfall over mass-weighted mean contributing distances of 0.3 to 2.1 km, and upwind source areas can exceed 3 km^2. Interbasin snow transport augments local snowfall by at least 23% in a first-order stream catchment (2 km^2), with the upwind “snowshed” doubling the effective catchment area. Snow imported across topographic divides is equivalent to 7% of annual streamflow in a 125 km^2 watershed. Kilometer-scale snow transport mediates alpine hydrology by permitting deep drift formation and augmenting the catchment water balance.

Plain Language Summary

Deep snow drifts represent a large amount of water concentrated into a small area, in contrast to precipitation, which is spatially smoother. Wind and avalanches can transport snow in mountain environments, concentrating relatively homogeneous snowfall into deep drifts. Snowfall must be accumulated over a relatively large area, and travel a long distance, to account for the amount of water stored in deep snow accumulation zones. I estimate a lower bound on snow transport with a new method that combines machine learning, snow modeling, and remote sensing. The results show that snowfall must accumulate over several kilometers to create observed drift patterns. Additionally, large amounts of snow can blow across mountain ridges, which has the effect of importing extra precipitation into downwind watersheds.

1 Introduction

Mountain snowpacks are a global water resource (Viviroli et al., 2007; Li et al., 2017), and the spatial distribution of snow mediates streamflow, soil moisture, and ecohydrology (Luce et al., 1998; Litaor et al., 2008; Williams et al., 2009; Wigmore & Molotch, 2024). Snowpack patterns are notoriously challenging to quantify (Dozier et al., 2016) due to process complexity (e.g., wind turbulence: Musselman et al., 2015) and the 10^8 range of relevant scales (Sturm, 2015).

Processes controlling the deposition and redistribution of alpine snow (Figure 1) are intensely studied at the scale of individual ridges and small catchments (e.g., Hiemstra et al., 2006; Lehning et al., 2008; Farinotti et al., 2010; Mott et al., 2010; Naaim-Bouvet et al., 2010; Mott et al., 2014; Walter et al., 2020). However, the scale-emergent effects of snow transport are more newly explored (Marsh et al., 2024; Quéno et al., 2024). Landscape-scale simulations commonly assume sub-kilometer fetch distances with suspension capped ~5 m above ground (Pomeroy et al., 1993; Marsh et al., 2020a). However, some regions exhibit multi-kilometer fetch distances (Figure 1A) with snow plumes extending hundreds of meters (Figure 1B). Some models can produce plumes (Groot Zwaaftink et al., 2011), but the attendant high-resolution wind fields complicate large-scale applications (Mott & Lehning, 2010; Schneiderbauer & Prokop 2011). Most models do not track snow, with the exception of Lagrangian particle tracking of preferential deposition (Wang & Huang, 2016).

The contributing distances and source areas of snow drifts have been studied for decades (Adok, 1977), but typically not in alpine environments. Early snow fence studies suggest contributing distances of ~1-3 km (Komarov, 1954; Tabler, 1971). From semi-empirical sublimation equations, Tabler and Schmidt (1973) infer a transport limit of 457-1421 m, sensitive to wind speed (assumed 12 m/s) and particle size. Snow accumulated from extensive alpine plateaus clearly contributes to “drift glaciers” (Olyphant, 1985; Hoffman et al., 2007; McGrath, 2022). Outcalt and MacPhail (1965) estimate that a ~0.1 km^2 drift glacier could collect snow from a ~1.3 km^2 source area by visual delimitation of topography and treeline. However, few if any studies have attempted to map drift source areas in comparable environments over the past 60 years.

Novel methods are needed to learn from patterns in remotely sensed snow data (Dozier, 2011; Sturm, 2015). I leverage differentiable modeling (Shen et al., 2023) to learn the fraction of snow exported from grid cells to their downwind neighbors (Figure 1). By tracking snow parcels through the trained model, I address two questions: (1) what contributing distances and source areas are necessary to explain alpine snow accumulation patterns, and (2) how might snow transport across topographic divides influence the catchment water balance?

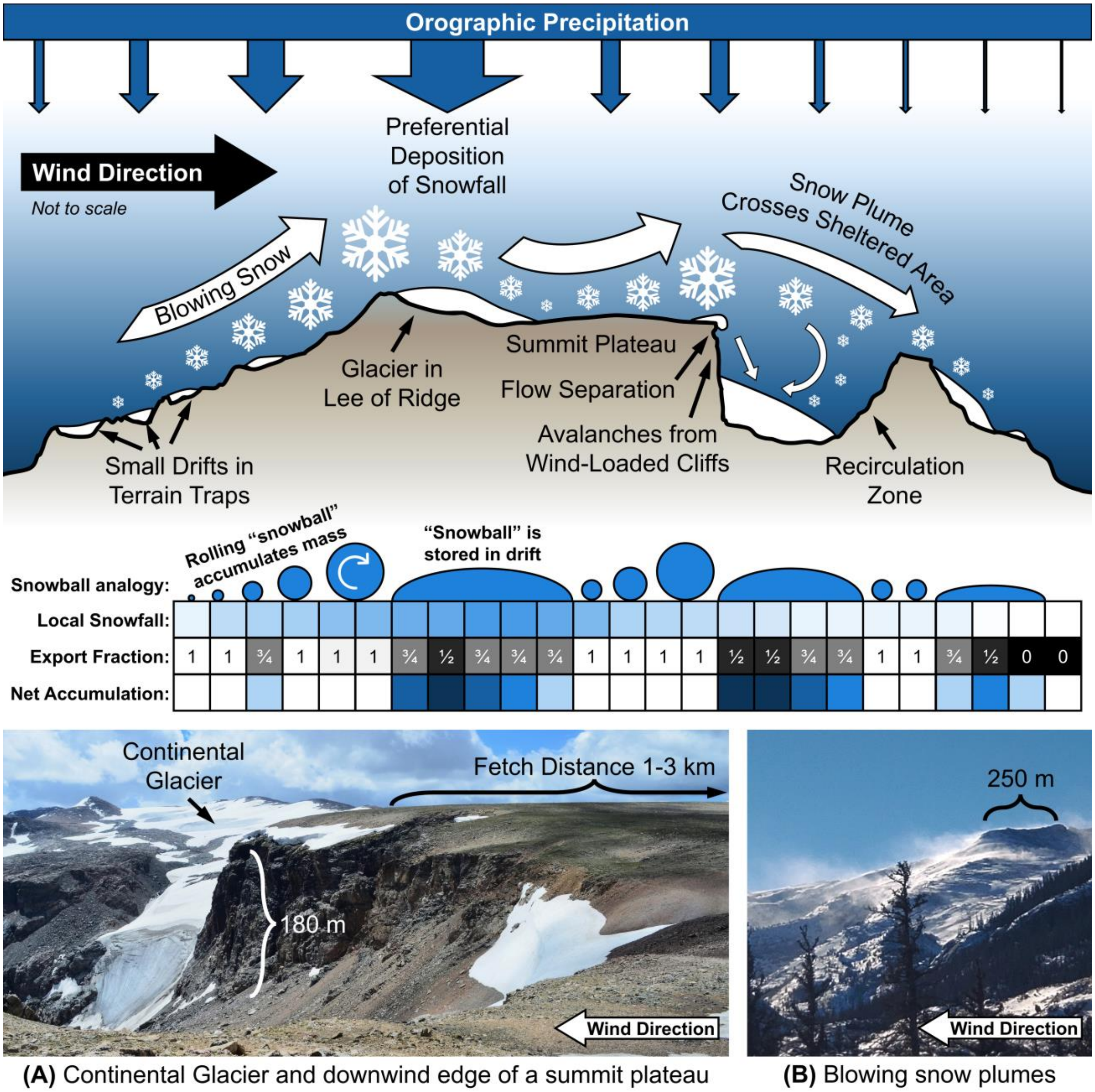

Figure 1. Conceptual model and study area photos. Snow transport processes are reduced to the export fraction between cells. By analogy, a "snowball" accumulates snow from areas with high export fractions and deposits snow in areas with low export fractions.

2 Methodology

In a three-part framework (Figure S2), I first estimate local snowfall and net accumulation with remote sensing and a process-based model. Second, I constrain snow transport by learning export fractions between grid cells. Third, I track snow parcels through the transport model.

2.1 Study Area and Data

I demonstrate this method in the Wind River Range, Wyoming (WRR). Anderson (2002) uses the WRR as the type locality for alpine plateau surfaces, a feature of mountain ranges globally (Calvet et al., 2015). Multi-kilometer wind fetch distances on these summit plateaus (Figure 1A) can produce deep drifts that mediate glaciation and streamflow (Boardman et al., in prep.).

Airborne lidar and hyperspectral data were acquired in the WRR on May 31, 2024, by Airborne Snow Observatories (ASO: Painter et al., 2016) in conjunction with backcountry fieldwork to constrain density variations (Boardman et al., in prep.). The final snow water equivalent (SWE) map is aggregated to 100 m resolution to highlight landscape-scale patterns, and an area outside lidar coverage is imputed (Figure S1, analogous to Appendix B of Boardman et al., in prep.).

2.2 Snow Modeling

The lidar-based “reference SWE map” reflects accumulation as well as patterns of interception, melt, and sublimation. A simple snow mass and energy balance model such as the two-layer snowpack sub-model of the Distributed Hydrology Soil Vegetation Model (DHSVM) can account for many of these processes and estimate seasonal accumulation (Wigmosta et al., 1994).

2.2.1 Setup and Calibration

DHSVM land surface parameters are from LANDFIRE (2022) and RCMAP (Rigge et al., 2021). Meteorological data from gridMET (Abatzoglou, 2013) are disaggregated with MetSim (Bennett et al., 2020). Modeled snowfall is distributed in proportion to the reference SWE map or uniformly below the lidar snowline. This multiplier-based approach implicitly accounts for preferential deposition and redistribution (Jackson, 1994; Vögeli et al., 2016).

Parameters are based on Sun et al. (2019) and refined by calibration, along with temperature and precipitation biases. Four objectives constrain model behavior: SWE root mean square error (RMSE); SWE R^2 for cells with SWE >1 m; SWE volume bias; and albedo RMSE for cells with SWE >0.1 m (from ASO hyperspectral data). Calibration is implemented using multi-objective Bayesian optimization (Emmerich et al., 2008).

The selected parameter set has SWE R^2 = 0.991 for cells with SWE >1 m. Exceptional model skill is possible because the reference SWE pattern is used to distribute snowfall. The calibrated model is Pareto-efficient across objectives (SWE RMSE = 0.12 m, volume bias = +8.8%, albedo RMSE = 0.26).

2.2.2 Snowfall and Accumulation

I estimate net accumulation by accounting for ablation in the lidar-based SWE map: "reference accumulation" = reference SWE + (modeled accumulation – modeled SWE). DHSVM indicates maximum SWE around May 10-15, 2024, with a 3% reduction by the May 31 survey, so the adjustment between SWE and seasonal accumulation is minor.

I model local snowfall in DHSVM assuming a smoother precipitation distribution. Orographic effects and preferential deposition control alpine snowfall (Lehning et al., 2008, Mott et al., 2018) at scales below the 4 km resolution of gridMET data. I infer a plausible above-ground snowfall pattern with a 2 km moving-average of the lidar-based pattern, applied twice to remove edge artifacts. The 2 km kernel preserves mountain-scale patterns while removing drifts. A smaller window preserves obvious drift patterns, which is disallowed. I also test three alternative patterns: (1) a 4 km moving-average, (2) Lanczos spline interpolation of gridMET precipitation, and (3) a uniform distribution. The 2 km kernel preserves the most spatial heterogeneity, so I use this snowfall pattern to estimate a lower bound on required transport and test sensitivity with the other patterns.

2.3 Differentiable Snow Transport Model

I develop a differentiable model of snow transport based on a feed-forward neural network, or NN (Caterini & Chang, 2018). Mass conservation and flux continuity are enforced. Unlike typical "black box" NN applications, learned weights physically represent the fraction of available snow exported from each grid cell (Figure 1).

2.3.1 Mathematical Structure

Assume an (x, y) model grid, size (m, n), with the prevailing wind direction toward increasing x. Each grid cell corresponds to a single neuron (Figure S2), with m "layers" (map columns) each containing n "neurons" (grid cells). Equation 1 defines transport:

$$A_x = W_x A_{x-1} + b_x = \begin{bmatrix} w_{1,1}^x & \cdots & w_{1,n}^x \\ \vdots & \ddots & \vdots \\ w_{n,1}^x & \cdots & w_{n,n}^x \end{bmatrix} \begin{bmatrix} a_1^{x-1} \\ \vdots \\ a_n^{x-1} \end{bmatrix} + \begin{bmatrix} b_1^x \\ \vdots \\ b_n^x \end{bmatrix} \tag{1}$$

The linear activation (A_x) represents the total available mass from local snowfall and incoming transport. First and last layer activations are zero to enforce no-transport boundaries. The bias (b_x) defines the local snowfall, and the weights matrix (W_x) defines the fraction of A_x transported between layers x-1 and x. Weights are scaled so that the export fraction (F_x) preserves mass:

$$F_x = \sum_i w_{i,j}^{x+1}, \quad 0 \le F_x < 1 \tag{2}$$

To enforce flux continuity, only tridiagonal entries of W_x are nonzero, so that snow from (x, y) can only arrive at (x+1, y) and (x+1, y±1). Dispersion occurs when snow is split between two downwind cells.

Only one of $w^x_{j+1,j}$ or $w^x_{j-1,j}$ may be significantly nonzero, thereby encoding a center-of-mass (COM) deflection angle at each cell. Following Figure S3, the maximum COM deflection angle (θ_{max}) is constrained by the ratio between lateral and diagonal transfer fractions:

$$w^x_{j\pm1,j} \le w^x_{j,j} * \frac{\tan(\theta_{max})}{1 - \tan(\theta_{max})} \tag{3}$$

The mass flux (Q_x) is defined by A_x and F_x, where $\odot$ denotes element-wise multiplication:

$$Q_x = F_x \odot A_x = W_x A_x \tag{4}$$

The net accumulation (N_x) is the residual of A_x and Q_x:

$$N_x = (A_x - Q_x) = (1 - F_x) \odot A_x \tag{5}$$

The distance-weighted mass flux (Q_{dist}) is analogous to the mean of Q_x, except that diagonal transport is scaled by $\sqrt{2}$ using distance matrix D:

$$Q_{dist} = \frac{1}{n * m} \sum_{x,y} (D \odot W_x) A_x \tag{6}$$

2.3.2 Training

The network learns transport pathways between the modeled above-ground snowfall and reference ground accumulation patterns. The reference accumulation pattern defines the sole training example, and the NN is not intended for generalized prediction since W_x encodes the site-specific spatial arrangement of scour and deposition zones. An error tolerance is required relative to the reference accumulation pattern due to uncertainty in the modeled snowfall.

The transport flux is equifinal, e.g., snow imported to (x, y) could come from (x-1, y) or (x-2, y), but a lower bound on transport can be estimated by minimizing Q_{dist}. Energy is dissipated roughly in proportion to distance traveled per unit mass (i.e., from friction), so minimizing Q_{dist} implies a lower bound on energy available for transport. Individual particles might follow longer paths, but minimizing Q_{dist} constrains the "path of least resistance" between local snowfall and net accumulation patterns.

2.3.3 Implementation

At 100 m resolution, the 442 km^2 study area requires 260 NN layers, each with 170 neurons. Prevailing westerly winds in the WRR are naturally oriented to the grid; elsewhere, a rotation may be necessary. The COM deflection angle is constrained to ±22.5°, consistent with drift patterns observed in the snow lidar data. With three valid weights per neuron, the NN has 132,090 learnable parameters (last layer fixed to zero).

Three constraints define an error tolerance, subject to which Q_{dist} is minimized. The predicted accumulation pattern must have RMSE <8 cm, which is the lowest error tolerance that does not cause unphysical aberrations (e.g., overfitting causes unrealistically high transport in forested areas). To reduce spatial biases, the error of each cell may not exceed 200% of the overall RMSE, i.e., ±16 cm. To reduce depth-dependent biases, cells are binned by accumulation depth in 10 cm increments, and the mean absolute bias across all bins may not exceed 1 cm.

Training is implemented in PyTorch (Paszke et al., 2019) using automatic differentiation (Baydin et al., 2017) and the Adam optimizer (Kingma & Ba, 2017) for 10^5 iterations. Training takes ~1.5 days on a consumer GPU.

2.4 Parcel Tracking

Mobile snow (Q_x) is assumed to be well-mixed within each cell. However, the total available snow (A_x) is not necessarily well-mixed, since transport may occur above a relatively immobile ground snowpack. To estimate a lower bound on transport, I assume that local snowfall contributes as much as possible of the net accumulation in each cell (Figure S4).

For each cell with net export (snowfall > accumulation), I propagate its contribution through the NN and track its contribution to all downwind cells. I then calculate the mean mass-weighted contributing distance of net accumulation in each cell (including local snowfall with zero distance). I also calculate the fraction of accumulation originating within a given upwind distance and the number of upwind cells that contribute at least 1, 10, or 100 mm of their local snowfall to a given downwind cell. Finally, I track how much snowfall from each cell ends up within specific watershed masks.

3 Results and Discussion

3.1 Snow Transport Flux

Figure 2 illustrates the northern WRR study area. The modeled 2024 seasonal snowfall is 0.42 m averaged across the domain, reaching 1.1 m at high elevations. Very deep accumulation zones (3-5.4 m SWE) contain 3-9 times more water than the local snowfall at those locations. The minimized distance-weighted mass flux is 0.91 m SWE per grid cell (Q_{dist}, Eq. 6), slightly higher than the mean flux of 0.80 m (Q_x, Eq. 4) due to diagonal transport. Q_x can reach 8-14 m at downwind plateau margins. Note that Q_x represents transport over an entire accumulation season, not an instantaneous flux.

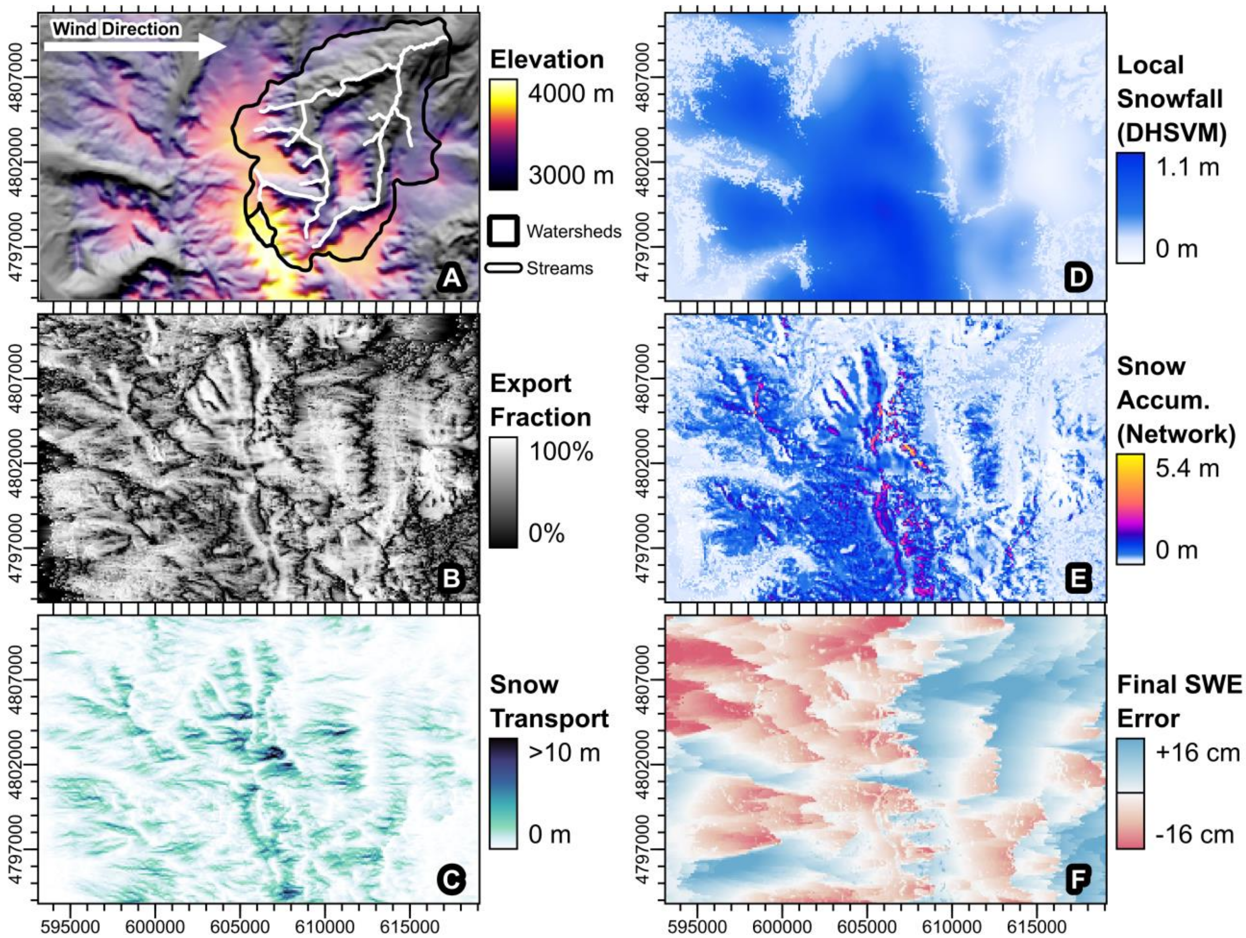

Figure 2. Study area maps: (A) shaded relief colored by elevation; (B) export fraction, F_x; (C) transport flux, Q_x; (D) local snowfall modeled by DHSVM, b_x; (E) net snow accumulation from the neural network, N_x; (F) error in final modeled SWE relative to measurements.

Higher export fractions (F_x, Eq. 2) are associated with summit plateaus, and lower export fractions define sheltered areas (Figure 2B). The median upwind shelter angle (Winstral & Marks 2002) is 2° for cells that export at least 0.5 m of SWE, and 15°, 20°, or 29° for cells that import at least 0.5, 1, or 2 m of SWE. Based on the WindNinja Reynolds-Averaged Navier-Stokes solver (Wagenbrenner et al., 2019), the median transport flux is 0.42 m in areas with lower-quartile wind speeds and 0.72 m (71% higher) in areas with upper-quartile wind speeds (Figure

S5). Despite lacking any explicit process representation or topographic input data, the NN implies sensible relationships between terrain, wind, and snow transport.

After accounting for ablation effects (Section 2.2.2), the NN matches the reference SWE map with $R^2 = 0.96$. Residual errors appear related to missing orographic effects and blowing snow sublimation (Figure 2F). Since errors are constrained to ±16 cm with no depth-dependent bias (Section 2.3.3), these errors should minimally impact analysis of the seasonal flux into cells with SWE >1 m. Indeed, by minimizing Q_{dist}, spatial biases in the residual error have the effect of underestimating transport, a desirable property for the lower bound estimated here.

3.2 Contributing Distance and Source Areas

The mass-weighted mean contributing distance over the whole study area is 0.15 km, increasing to 0.43 km for cells with SWE >1 m and 0.92 km for SWE >3 m (Figure 3A). Local snowfall exceeds net accumulation for 86% of cells with SWE <1 m. However, cells with SWE >1 m import 46% of their net accumulation, and the upwind contributing distance increases rapidly for deep drift zones (Figure 3B). The fraction of net accumulation imported from >1 km upwind increases from 14% for cells with 1-2 m SWE to 21%, 32%, 44%, and 53% for successively deeper SWE bins (1 m increments). For 100 m cells with 4-6 m SWE (N = 13), 47% of net accumulation is imported from >1 km upwind, and 15% is from >2 km upwind.

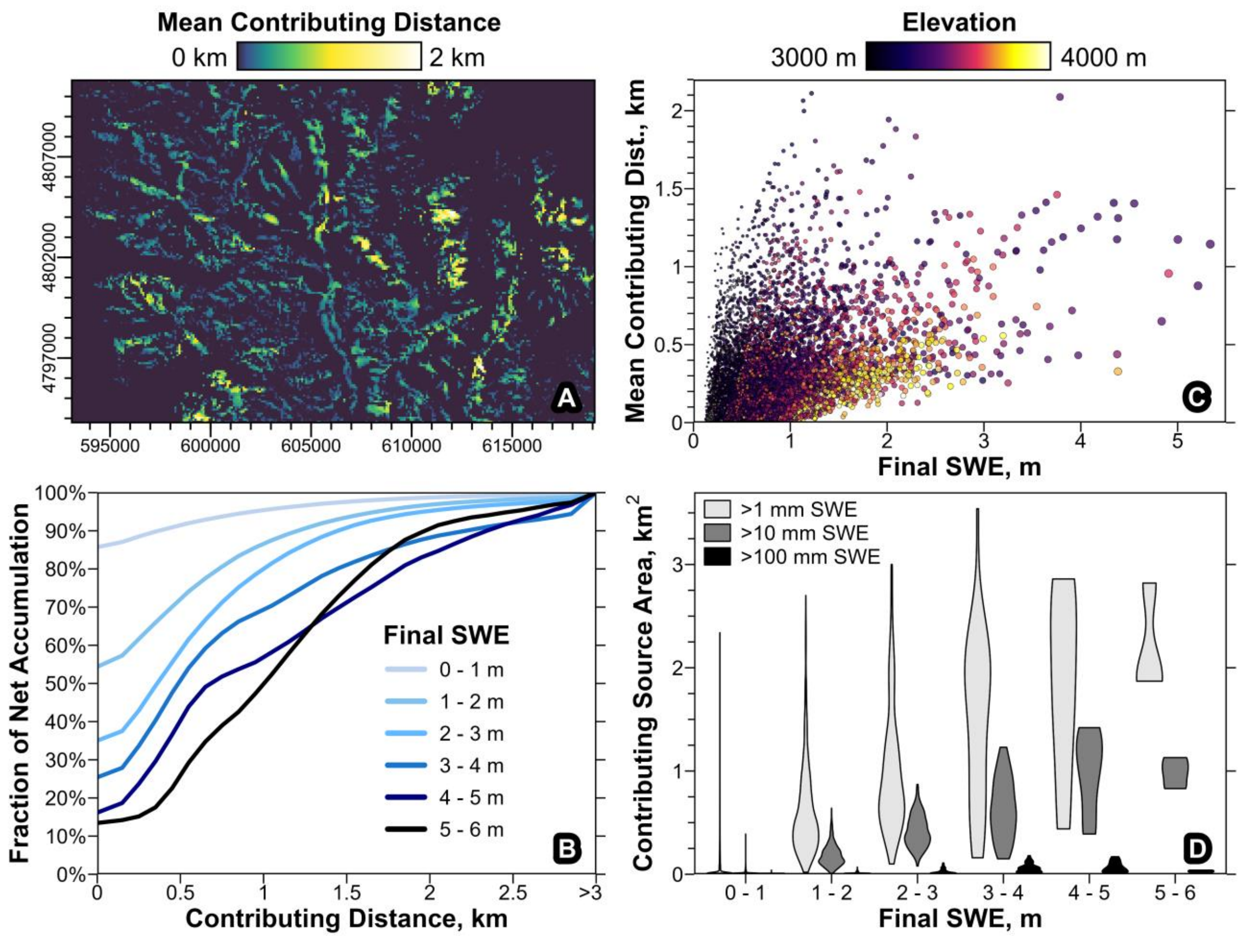

Figure 3. (A) Map of mass-weighted mean contributing distance; (B) fraction of net accumulation that originates within a given distance upwind, binned by final SWE; (C) final SWE vs. mean contributing distance for each grid cell, colored by elevation; (D) distribution of contributing source areas from which at least 1, 10, or 100 mm of local snowfall is imported to a given downwind cell, binned by final downwind SWE.

The relationship between contributing distance and final SWE depth is nuanced (Figure 3C), with Pearson correlation r = 0.59. The mean contributing distance varies from 0.3 to 2.1 km for SWE >3 m. Drifts covering a larger area require longer contributing distances compared to isolated drifts. Long-distance transport is also associated with deep snow at relatively low elevations due to reduced local snowfall. For example, there is an r = -0.41 correlation between elevation and contributing distance for cells with 1-2 m SWE. The longest mean contributing distances (1.9-2.1 km) are associated with relatively low elevations (3200-3400 m) and medium to deep SWE (1-4 m) along the downwind margins of summit plateaus.

Most deep snow is accumulated incrementally from a relatively large source area (Figure 3D). Two notable cirques collect snowfall from 2.8-3.5 km^2 contributing source areas. The median source area contributing at least 1 mm of SWE to a given downwind cell is 0.9 km^2 for downwind cells with SWE >2 m and 1.8 km^2 for SWE >3 m. Source areas shrink when raising the minimum contribution threshold, with a median of 1.8, 0.7, or 0.04 km^2 contributing >1, >10, or >100 mm to cells with SWE >3 m. There is a negative correlation (r = -0.76, N = 49) between the size of areas contributing >1 or >100 mm to cells with SWE >3 m. Concentrated transport (>100 mm imported from each cell in a >0.1 km^2 area) produces deep accumulation (2.8-4.8 m SWE) with an abnormally low mean contributing distance of 0.41 km, compared to 0.83 km across all cells in the same accumulation range. The topographic setting of these concentrated transport areas (steep headwalls) suggests a dominant role of avalanches. The stratification of concentrated and dispersed source areas might help classify dominant snow transport processes.

3.3 Snowshed Boundaries

Snow transport across topographic divides complicates the concept of catchment area. Two streams are gauged in the study area: Torrey Creek (125 km^2), monitored continuously by the author, and a meltwater stream from the upper Continental Glacier (2.0 km^2), monitored intermittently by Vandeberg and VanLooy (2016, 2024). Figure 4 illustrates the “snowshed” boundaries of these streams, defined here as the area from which some fraction of snowfall may contribute to streamflow at a specified pour point. Snowsheds overlap between watersheds because import/export areas also retain some local snowfall. Moreover, snowsheds are spatially discontinuous due to intervening sheltered areas (i.e., snow may blow over a sheltered gully).

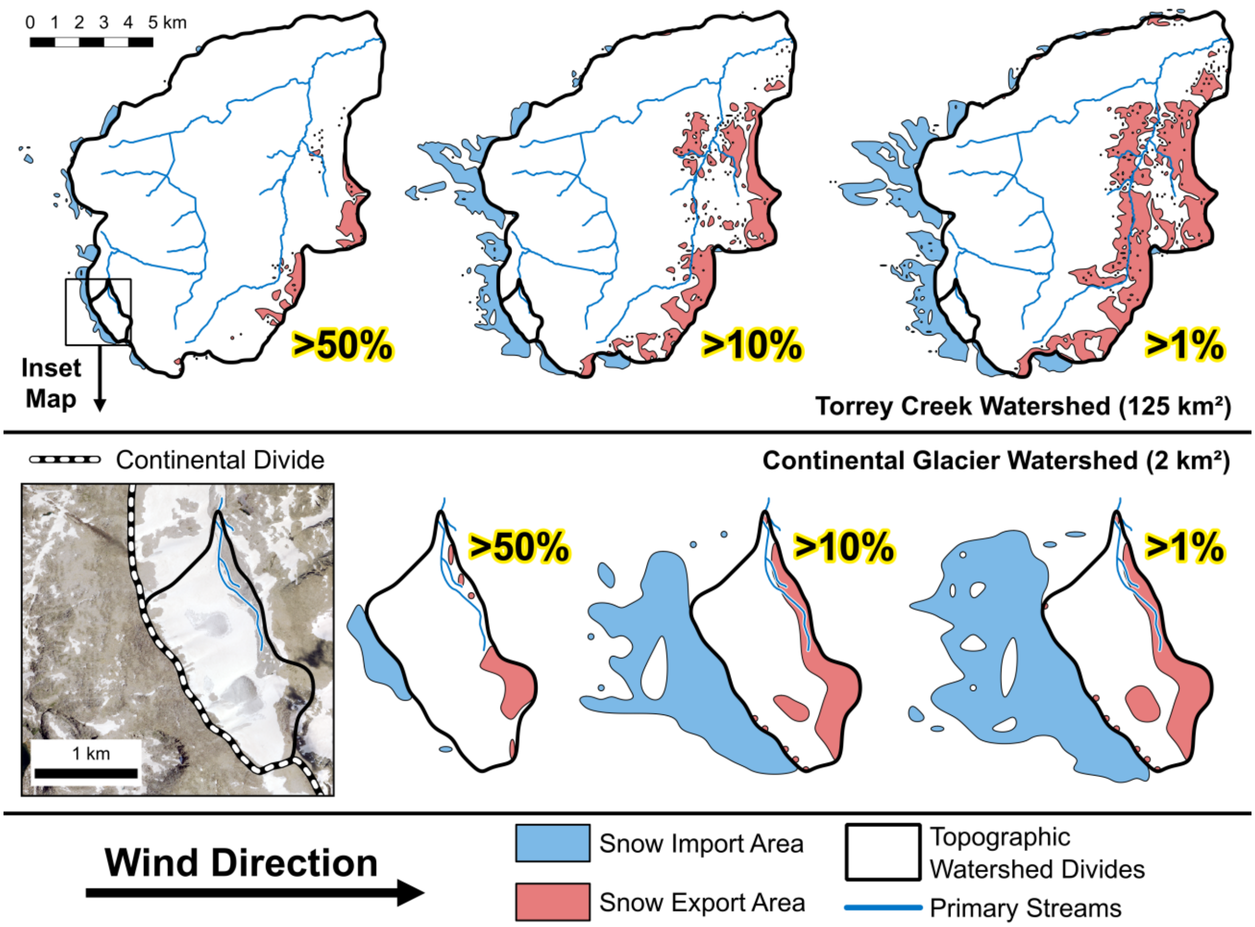

Figure 4. "Snowshed" boundaries for the Torrey Creek and Continental Glacier watersheds (locations in Figure 2A). Colored polygons represent areas where at least 50%, 10%, or 1% of the local snowfall is imported into or exported out of the watershed. Imagery: NAIP, July 2022.

The effective Torrey Creek catchment increases by 16 km^2 (13%) when including areas that contribute >1% of local snowfall. Conversely, an interior area of 23 km^2 (18%) exports >1% of local snowfall out of the watershed. Although the export area is larger than the import area, snowfall is higher along the WRR crest. Thus, Torrey Creek imports 6.6% of its accumulation and only exports 2.8%, producing a net gain of 1.6 cm watershed-average SWE.

The difference between snowshed and watershed boundaries is most pronounced at smaller scales. About 23% of snow accumulation in the Continental Glacier first-order stream catchment originates outside the topographic watershed, which is a lower bound that assumes a maximal contribution from direct snowfall on the glacier (Section 2.4). The effective catchment area more than doubles (2.0 to 4.4 km^2) when including areas that contribute >1% of local snowfall (Figure 4). The patch of modeled snowfall export from the Continental Glacier aligns with observed bare ice patches caused by early ablation of the thin residual snowpack (VanLooy et al., 2013).

There is a considerable flux of snow across the Continental Divide from Pacific to Atlantic basins (~3x10^5 kg/m seasonally). The total mass imported into Torrey Creek (largely across the Continental Divide) is 3.5×10^{-3} km^3, equivalent to 7% of the 2024 water yield. Over the October-May accumulation season, this equates to a mean snow transport flux of 0.17 m^3/s entering the watershed, or 32% of mean streamflow on the same time period. Baker (1946) first hypothesized that snow drifting across the Continental Divide might underlie patterns of glacier abundance in the WRR. The present results support a sizable impact of interbasin snow transport on watershed-scale snow accumulation patterns.

3.4 Sensitivity and Interpretation

The baseline 2 km moving average snowfall pattern provides a conservative lower bound on transport by preserving considerable heterogeneity in the local snowfall pattern. With the alternative snowfall patterns (Section 2.2.2), the contributing distance for cells with SWE >3 m increases by 17-41% and the interbasin flux into Torrey Creek increases by 24-53% (Table S1). While the true transport flux remains uncertain, multi-kilometer transport is an important control on snow accumulation patterns in all scenarios. The relationships between topography, SWE, contributing distance, and snowshed boundaries also remain reasonably consistent (Figure S6-S8).

Minimizing Q_{dist} (Section 2.3.2) causes each snow parcel to move directly towards its final destination, unlike real-world blowing snow, which is turbulent and undirected. Again, this approach leads to a conservative lower bound on contributing distances since the modeled snow “knows” where to go, unlike real snow.

It is challenging to separate transport into preferential deposition and redistribution, and these results might partially represent near-surface snowfall dynamics. However, my treatment is similar to process-based transport models that account for preferential deposition by re-suspending snowfall after it reaches the ground (cf. Reynolds et al., 2021, Section 6.4). Scipión et al. (2013) confirm that snowfall several hundred meters above ground is much smoother than ground snow accumulation patterns. Transport fluxes described here are best interpreted relative to snowfall above the near-surface flow field (Mott et al., 2018).

Although physically constrained by mass conservation and flux continuity, the NN is highly abstracted and lacks sublimation processes. However, self-limiting humidity feedbacks may reduce alpine sublimation to ~0.1% of precipitation (Groot Zwaaftink et al., 2013). Quéno et al. (2024) similarly found that transport outweighs sublimation in shaping landscape-scale alpine snow patterns. Still, future work could potentially include sublimation in the differentiable modeling framework.

4 Conclusions

Assuming that precipitation patterns are considerably smoother, the WRR snowpack distribution results from multi-kilometer transport. Extensive areas of SWE >3 m (3-9 times seasonal snowfall) imply contributing distances of 0.3-2.1 km with drift source areas up to 3.5 km^2. Due to large interbasin transport fluxes, snowsheds may be more relevant than purely topographic watersheds for understanding streamflow generation in windy and snowy environments.

The framework described here is an example of differentiable modeling, a burgeoning field in the geosciences (Shen et al., 2023). The structure of neural networks makes them well-suited for representing directional transport, which could extend to many other hydrological processes.

Acknowledgements

I acknowledge ownership of Mountain Hydrology LLC, which funded snow data acquisition under Bureau of Reclamation award R24AC00025-00. I am grateful to my PhD committee and especially Adrian Harpold and Mark Wigmosta for years of modeling guidance and encouragement on my side projects.

Open Research

Data, processing scripts, and DHSVM model source code necessary to reproduce figures and numerical results from this study are publicly archived at Boardman (2024a). In addition to inclusion in the archive (Boardman 2024a), the modified version of DHSVM used for this study is also developed publicly on GitHub (Boardman, 2024b). Lidar and hyperspectral data products acquired commercially by Airborne Snow Observatories, Inc. (ASO) are excluded from the archive due to contractual license restrictions but can be publicly accessed from the ASO data portal (Airborne Snow Observatories, 2024).

References

Abatzoglou, J. T. (2013). Development of gridded surface meteorological data for ecological applications and modelling. *International Journal of Climatology*, *33*(1), 121–131. https://doi.org/10.1002/joc.3413

Adok, U. (1977). Snow Drift. *Journal of Glaciology*, *19*(81), 123–139. https://doi.org/10.3189/S0022143000215591

Airborne Snow Observatories, Inc. (2024). *ASO_NorthernWindRivers_2024May31_AllData_and_Reports* [Dataset]. https://data.airbornesnowobservatories.com/

Anderson, R. S. (2002). Modeling the tor-dotted crests, bedrock edges, and parabolic profiles of high alpine surfaces of the Wind River Range, Wyoming. *Geomorphology*, *46*(1–2), 35–58. https://doi.org/10.1016/S0169-555X(02)00053-3

Baker, C. L. (1946). Geology of the Northwestern Wind River Mountains, Wyoming. *Geological Society of America Bulletin*, *57*(6), 565–596. https://doi.org/10.1130/0016-7606(1946)57[565:GOTNWR]2.0.CO;2

Baydin, A. G., Pearlmutter, B. A., Radul, A. A., & Siskind, J. M. (2017). Automatic differentiation in machine learning: A survey. *J. Mach. Learn. Res.*, *18*(1), 5595–5637.

Bennett, A., Hamman, J., & Nijssen, B. (2020). MetSim: A Python package for estimation and disaggregation of meteorological data. *Journal of Open Source Software*, *5*(47), 2042. https://doi.org/10.21105/joss.02042

Boardman, E. (2024a). *Dataset for Snow Transport Modeling in the Northern Wind River Range* [Dataset]. Zenodo. https://doi.org/10.5281/zenodo.14201720

Boardman, E. (2024b). *Eli-mtnhydro/DHSVM-MtnHydro* [Software]. https://github.com/eli-mtnhydro/DHSVM-MtnHydro

Calvet, M., Gunnell, Y., & Farines, B. (2015). Flat-topped mountain ranges: Their global distribution and value for understanding the evolution of mountain topography. *Geomorphology*, *241*, 255–291. https://doi.org/10.1016/j.geomorph.2015.04.015

Caterini, A. L., & Chang, D. E. (2018). *Deep Neural Networks in a Mathematical Framework*. Springer International Publishing. https://doi.org/10.1007/978-3-319-75304-1

Dozier, J. (2011). Mountain hydrology, snow color, and the fourth paradigm. *Eos, Transactions American Geophysical Union*, *92*(43), 373–374. https://doi.org/10.1029/2011EO430001

Dozier, J., Bair, E. H., & Davis, R. E. (2016). Estimating the spatial distribution of snow water equivalent in the world's mountains. *WIREs Water*, *3*(3), 461–474. https://doi.org/10.1002/wat2.1140

Earth Resources Observation And Science (EROS) Center. (2017). *National Agriculture Imagery Program (NAIP), images: M_4310943_ne_12_060_20220710 and m_4310943_nw_12_060_20220717* [Tiff]. U.S. Geological Survey. https://doi.org/10.5066/F7QN651G

Emmerich, M., Deutz, A., & Klinkenberg, J.-W. (2008). The computation of the expected improvement in dominated hypervolume of Pareto front approximations. *Leiden Institute for Advanced Computer Science*. https://liacs.leidenuniv.nl/~emmerichmtm/moda/material/TR-ExI.pdf

Farinotti, D., Magnusson, J., Huss, M., & Bauder, A. (2010). Snow accumulation distribution inferred from time-lapse photography and simple modelling. *Hydrological Processes*, *24*(15), 2087–2097. https://doi.org/10.1002/hyp.7629

Groot Zwaaftink, C. D., Löwe, H., Mott, R., Bavay, M., & Lehning, M. (2011). Drifting snow sublimation: A high-resolution 3-D model with temperature and moisture feedbacks. *Journal of Geophysical Research: Atmospheres*, *116*(D16). https://doi.org/10.1029/2011JD015754

Groot Zwaaftink, C. D., Mott, R., & Lehning, M. (2013). Seasonal simulation of drifting snow sublimation in Alpine terrain. *Water Resources Research*, *49*(3), 1581–1590. https://doi.org/10.1002/wrcr.20137

Hiemstra, C. A., Liston, G. E., & Reiners, W. A. (2006). Observing, modelling, and validating snow redistribution by wind in a Wyoming upper treeline landscape. *Ecological Modelling*, *197*(1), 35–51. https://doi.org/10.1016/j.ecolmodel.2006.03.005

Hoffman, M. J., Fountain, A. G., & Achuff, J. M. (2007). 20th-century variations in area of cirque glaciers and glacierets, Rocky Mountain National Park, Rocky Mountains, Colorado, USA. *Annals of Glaciology*, *46*, 349–354. https://doi.org/10.3189/172756407782871233

Jackson, T. H. R. (1994). *A spatially distributed snowmelt-driven hydrologic model applied to the upper Sheep Creek watershed* [PhD Dissertation, Department of Civil and Environmental Engineering, Utah State University]. https://www.proquest.com/dissertations-theses/spatially-distributed-snowmelt-driven-hydrologic/docview/304120742/se-2

Kingma, D. P., & Ba, J. (2017). *Adam: A Method for Stochastic Optimization* (arXiv:1412.6980). arXiv. https://doi.org/10.48550/arXiv.1412.6980

Komarov, A. A. (1954). Some rules on the migration and deposition of snow in Western Siberia and their application to control measures (G. Belkov, Trans.). In *Technical Translation (National Research Council of Canada): Vol. NRC-TT-1094* (NRC-TT-1094,). National Research Council of Canada. https://doi.org/10.4224/20331553

LANDFIRE. (2022). *LANDFIRE 2022 Existing Vegetation Type (EVT)* [Dataset]. U.S. Department of the Interior, Geological Survey, and U.S. Department of Agriculture. http://www.landfire/viewer

Lehning, M., Löwe, H., Ryser, M., & Raderschall, N. (2008). Inhomogeneous precipitation distribution and snow transport in steep terrain. *Water Resources Research*, *44*(7). https://doi.org/10.1029/2007WR006545

Li, D., Wrzesien, M. L., Durand, M., Adam, J., & Lettenmaier, D. P. (2017). How much runoff originates as snow in the western United States, and how will that change in the future? *Geophysical Research Letters*, *44*(12), 6163–6172. https://doi.org/10.1002/2017GL073551

Litaor, M. I., Williams, M., & Seastedt, T. R. (2008). Topographic controls on snow distribution, soil moisture, and species diversity of herbaceous alpine vegetation, Niwot Ridge, Colorado. *Journal of Geophysical Research: Biogeosciences*, *113*(G2). https://doi.org/10.1029/2007JG000419

Luce, C. H., Tarboton, D. G., & Cooley, K. R. (1998). The influence of the spatial distribution of snow on basin-averaged snowmelt. *Hydrological Processes*, *12*(10–11), 1671–1683. https://doi.org/10.1002/(SICI)1099-1085(199808/09)12:10/11<1671::AID-HYP688>3.0.CO;2-N

Marsh, C. B., Lv, Z., Vionnet, V., Harder, P., Spiteri, R. J., & Pomeroy, J. W. (2024). Snowdrift-Permitting Simulations of Seasonal Snowpack Processes Over Large Mountain Extents. *Water Resources Research*, *60*(8), e2023WR036948. https://doi.org/10.1029/2023WR036948

Marsh, C. B., Pomeroy, J. W., Spiteri, R. J., & Wheater, H. S. (2020). A Finite Volume Blowing Snow Model for Use With Variable Resolution Meshes. *Water Resources Research*, *56*(2), e2019WR025307. https://doi.org/10.1029/2019WR025307

McGrath, D. (2022). Blowing in the wind: The glaciers of Colorado. *Mountain Geologist*, *59*(3), 229–238. https://doi.org/10.31582/rmag.mg.59.3.229

Mott, R., & Lehning, M. (2010). Meteorological Modeling of Very High-Resolution Wind Fields and Snow Deposition for Mountains. *Journal of Hydrometeorology*, *11*(4), 934–949. https://doi.org/10.1175/2010JHM1216.1

Mott, R., Schirmer, M., Bavay, M., Grünewald, T., & Lehning, M. (2010). Understanding snow-transport processes shaping the mountain snow-cover. *The Cryosphere*, *4*(4), 545–559. https://doi.org/10.5194/tc-4-545-2010

Mott, R., Scipión, D., Schneebeli, M., Dawes, N., Berne, A., & Lehning, M. (2014). Orographic effects on snow deposition patterns in mountainous terrain. *Journal of Geophysical Research: Atmospheres*, *119*(3), 1419–1439. https://doi.org/10.1002/2013JD019880

Mott, R., Vionnet, V., & Grünewald, T. (2018). The Seasonal Snow Cover Dynamics: Review on Wind-Driven Coupling Processes. *Frontiers in Earth Science*, *6*. https://doi.org/10.3389/feart.2018.00197

Musselman, K. N., Pomeroy, J. W., Essery, R. L. H., & Leroux, N. (2015). Impact of windflow calculations on simulations of alpine snow accumulation, redistribution and ablation. *Hydrological Processes*, *29*(18), 3983–3999. https://doi.org/10.1002/hyp.10595

Naaim-Bouvet, F., Bellot, H., & Naaim, M. (2010). Back analysis of drifting-snow measurements over an instrumented mountainous site. *Annals of Glaciology*, *51*(54), 207–217. https://doi.org/10.3189/172756410791386661

Olyphant, G. A. (1985). Topoclimate and the Distribution of Neoglacial Facies in the Indian Peaks Section of the Front Range, Colorado, U.S.A. *Arctic and Alpine Research*, *17*(1), 69–78. https://doi.org/10.1080/00040851.1985.12004449

Outcalt, S. I., & MacPhail, D. D. (1965). A Survey of Neoglaciation in the Front Range of Colorado. *University of Colorado Studies, Series in Earth Sciences*, *4*, 124.

Painter, T. H., Berisford, D. F., Boardman, J. W., Bormann, K. J., Deems, J. S., Gehrke, F., Hedrick, A., Joyce, M., Laidlaw, R., Marks, D., Mattmann, C., McGurk, B., Ramirez, P., Richardson, M., Skiles, S. M., Seidel, F. C., & Winstral, A. (2016). The Airborne Snow Observatory: Fusion of scanning lidar, imaging spectrometer, and physically-based modeling for mapping snow water equivalent and snow albedo. *Remote Sensing of Environment*, *184*, 139–152. https://doi.org/10.1016/j.rse.2016.06.018

Paszke, A., Gross, S., Massa, F., Lerer, A., Bradbury, J., Chanan, G., Killeen, T., Lin, Z., Gimelshein, N., Antiga, L., Desmaison, A., Köpf, A., Yang, E., DeVito, Z., Raison, M., Tejani, A., Chilamkurthy, S., Steiner, B., Fang, L., … Chintala, S. (2019). *PyTorch: An Imperative Style, High-Performance Deep Learning Library* (arXiv:1912.01703). arXiv. https://doi.org/10.48550/arXiv.1912.01703

Pomeroy, J. W., Gray, D. M., & Landine, P. G. (1993). The Prairie Blowing Snow Model: Characteristics, validation, operation. *Journal of Hydrology*, *144*(1), 165–192. https://doi.org/10.1016/0022-1694(93)90171-5

Quéno, L., Mott, R., Morin, P., Cluzet, B., Mazzotti, G., & Jonas, T. (2024). Snow redistribution in an intermediate-complexity snow hydrology modelling framework. *The Cryosphere*, *18*(8), 3533–3557. https://doi.org/10.5194/tc-18-3533-2024

Reynolds, D. S., Pflug, J. M., & Lundquist, J. D. (2021). Evaluating Wind Fields for Use in Basin-Scale Distributed Snow Models. *Water Resources Research*, *57*(2), e2020WR028536. https://doi.org/10.1029/2020WR028536

Rigge, M. B., Bunde, B., Shi, H., & Postma, K. (2021). *Rangeland Condition Monitoring Assessment and Projection (RCMAP) Fractional Component Time-Series Across the Western U.S. 1985-2020* [Dataset]. U.S. Geological Survey. https://doi.org/10.5066/P95IQ4BT

Schneiderbauer, S., & Prokop, A. (2011). The atmospheric snow-transport model: SnowDrift3D. *Journal of Glaciology*, *57*(203), 526–542. https://doi.org/10.3189/002214311796905677

Scipión, D. E., Mott, R., Lehning, M., Schneebeli, M., & Berne, A. (2013). Seasonal small-scale spatial variability in alpine snowfall and snow accumulation. *Water Resources Research*, *49*(3), 1446–1457. https://doi.org/10.1002/wrcr.20135

Shen, C., Appling, A. P., Gentine, P., Bandai, T., Gupta, H., Tartakovsky, A., Baity-Jesi, M., Fenicia, F., Kifer, D., Li, L., Liu, X., Ren, W., Zheng, Y., Harman, C. J., Clark, M., Farthing, M., Feng, D., Kumar, P., Aboelyazeed, D., … Lawson, K. (2023). Differentiable modelling to unify machine learning and physical models for geosciences. *Nature Reviews Earth & Environment*, *4*(8), 552–567. https://doi.org/10.1038/s43017-023-00450-9

Sturm, M. (2015). White water: Fifty years of snow research in WRR and the outlook for the future. *Water Resources Research*, *51*(7), 4948–4965. https://doi.org/10.1002/2015WR017242

Sun, N., Yan, H., Wigmosta, M. S., Leung, L. R., Skaggs, R., & Hou, Z. (2019). Regional Snow Parameters Estimation for Large-Domain Hydrological Applications in the Western United States. *Journal of Geophysical Research: Atmospheres*, *124*(10), 5296–5313. https://doi.org/10.1029/2018JD030140

Tabler, R. D. (1971). Design of a Watershed Snow Fence System, and First-Year Snow Accumulation. *Proceedings of the 39th Annual Western Snow Conference*, 50–55.

Tabler, R. D., & Schmidt, R. A. (1973). Weather conditions that determine snow transport distances at a site in Wyoming. In *The role of snow and ice in hydrology* (Vol. 1, pp. 118–127). Proceedings of the Banff Symposia.

Vandeberg, G. S., & VanLooy, J. A. (2016). Continental Glacier meltwater contributions to late summer stream flow and water quality in the northern Wind River Range, Wyoming, USA. *Environmental Earth Sciences*, *75*(5), 389. https://doi.org/10.1007/s12665-016-5295-0

VanLooy, J. A., Forster, R. R., Barta, D., & Turrin, J. (2013). Spatially variable surface elevation changes and estimated melt water contribution of Continental Glacier in the Wind River Range, Wyoming, USA: 1966–2011. *Geocarto International*, *28*(2), 98–113. https://doi.org/10.1080/10106049.2012.665500

VanLooy, J. A., & Vandeberg, G. S. (2024). Glacier Meltwater Impacts to Late Summer Flow and Geochemistry of Tributaries in the Wind River Range, Wyoming, USA. *The Professional Geographer*, *0*(0), 1–7. https://doi.org/10.1080/00330124.2024.2341073

Viviroli, D., Dürr, H. H., Messerli, B., Meybeck, M., & Weingartner, R. (2007). Mountains of the world, water towers for humanity: Typology, mapping, and global significance. *Water Resources Research*, *43*(7). https://doi.org/10.1029/2006WR005653

Vögeli, C., Lehning, M., Wever, N., & Bavay, M. (2016). Scaling Precipitation Input to Spatially Distributed Hydrological Models by Measured Snow Distribution. *Frontiers in Earth Science*, *4*. https://doi.org/10.3389/feart.2016.00108

Wagenbrenner, N. S., Forthofer, J. M., Page, W. G., & Butler, B. W. (2019). Development and Evaluation of a Reynolds-Averaged Navier–Stokes Solver in WindNinja for Operational Wildland Fire Applications. *Atmosphere*, *10*(11), Article 11. https://doi.org/10.3390/atmos10110672

Walter, B., Huwald, H., Gehring, J., Bühler, Y., & Lehning, M. (2020). Radar measurements of blowing snow off a mountain ridge. *The Cryosphere*, *14*(6), 1779–1794. https://doi.org/10.5194/tc-14-1779-2020

Wang, Z., & Huang, N. (2017). Numerical simulation of the falling snow deposition over complex terrain. *Journal of Geophysical Research: Atmospheres*, *122*(2), 980–1000. https://doi.org/10.1002/2016JD025316

Wigmore, O., & Molotch, N. P. (2024). Snow drifts as a driver of alpine plant productivity as observed from weekly multispectral drone imagery. *Ecohydrology*, *17*(7), e2694. https://doi.org/10.1002/eco.2694

Wigmosta, M. S., Vail, L. W., & Lettenmaier, D. P. (1994). A distributed hydrology-vegetation model for complex terrain. *Water Resources Research*, *30*(6), 1665–1679. https://doi.org/10.1029/94WR00436

Williams, C. J., McNamara, J. P., & Chandler, D. G. (2009). Controls on the temporal and spatial variability of soil moisture in a mountainous landscape: The signature of snow and complex terrain. *Hydrology and Earth System Sciences*, *13*(7), 1325–1336. https://doi.org/10.5194/hess-13-1325-2009